Ionizable copolymer functionalized magnetic nanocomposite as an adsorbent for boosting the extraction selectivity of aristolochic acids

Recommended Citation

Ionizable copolymer functionalized magnetic nanocomposite as an adsorbent for boosting the extraction selectivity of aristolochic acids

Qi-Yue Xie [a,1], Yang Chen [a,1], Chang-Jun Li [a], Jia-Bin Zhang [b], Xiu-Jun Cao [a,*], Jun Lu [a,**]

[a] State Key Laboratory of Southwestern Chinese Medicine Resources, School of Pharmacy, Chengdu University of Traditional Chinese Medicine, Chengdu, 611137, PR China
[b] Suzhou CretBiotech Ltd., 99 Jinji Lake Avenue, Suzhou, 215123 PR China

Abstract

Aristolochic acid nephropathy (AAN) has drawn increasing public attention. Organic anion transporters (OATs) are considered to be responsible for mediating nephrotoxicity of aristolochic acids (AAs), as AAs are typical OAT1 substrates that exhibit anionic properties and contain one hydrophobic domain. Inspired by the OAT1 three-dimensional structure or substrate/protein interactions involved in transport, we designed a magnetic polymeric hybrid, mimicking the effect of basic and aromatic residues of OAT1, for efficient enriching aristolochic acid I (AA I) and aristolochic acid II (AA II) in Traditional Chinese patent medicines (TCPM). N, N-dimethylaminopropyl acrylamide (DMAPAm) was used as a cationic monomer and copolymerized with divinylbenzene (DVB) onto the surface of monodisperse magnetic nanoparticles (denoted as MNs@SiO$_2$T-DvbDam). The magnetic polymer hybrid demonstrated high selectivity and capacity for AAs, which was mainly attributed to (1) electrostatic interactions from the cationic or basic moiety of DMAPAm and (2) the hydrophobic and π-π stacking interactions from the aromatic ring of DVB. Additionally, the surface of the hybrid exhibited amphiphilic property according to the ionization of DMAPAm, thus improving the compatibility of the adsorbent with the aqueous sample matrix. This strategy was proven to be robust in the analysis of real drug samples, which was characterized by a good linearity, high recovery and satisfactory reusability. This work confirmed that the proposed tool could be a promising candidate for enhancing the extraction selectivity of AAs in Traditional Chinese medicines (TCM).

Keywords: Amphiphilic, Aristolochic acids, Ionization, Magnetic copolymer, Traditional Chinese patent medicines

1. Introduction

Aristolochic acids (AAs) are a group of structurally related nitrophenanthrene carboxylic acid naturally produced in Aristolochic and Asarum plant species, which have been used worldwide as herbal medicine for centuries to treat inflammatory and infectious disorders [1–3] such as gastrointestinal complaints, fungal skin diseases, poisoning caused by a snake bite and so forth. However, it has been reported that AAs are closely associated with some diseases extremely like kidney failures [4–6]. It is further confirmed the rapidly progressive kidney fibrotic disease caused by high concentrations of AAs in the drugs is named as aristolochic acid nephrology (AAN). The nephrotoxic mechanism of AAs involves the abnormal cellular transport of anionic drugs of AAs by organic anion transporters (OATs) [7]. In addition, AAs are regarded as potent carcinogen for intrahepatic bile duct carcinomas in China [8] as well as liver carcinomas in southeast Asian countries [9]. Furthermore, AAs can interact with DNA, and the DNA adducts further disturb the metabolism pathways [10]. Many countries such as America, England and Germany severely restricted

the use of AAs [11]. Moreover, International Agency for Research on Cancer (IARC) listed AAs and related plants as group 1 carcinogens [12]. The Chinese Pharmacopoeia in 2020 definitely excluded high level AAs-containing herbs such as Ma-Dou-Ling (*Dutchmanspipe Fruit*) and Tian-Xian-Teng (*Aristolochiae Herba*). However, some AAs-containing herbs such as Xi-Xin were still allowed to use as important crude ingredients [13]. Considering potent toxicity of AAs and their possible exposure in drugs, it was imperative to establish highly sensitive and selective detection methods for AAs, especially aiming at AAs-containing Traditional Chinese patent medicines (TCPM) in the market.

Among the common detection methods, high performance liquid chromatography (HPLC) and liquid chromatography/mass spectrometry (LC/MS) provide a high separation efficiency and detection sensitivity [14−20]. Moreover, HPLC is more commonly used in the laboratory for the determination of AAs analogs due to its cost-effective property. One challenge with detecting AAs at low abundance is huge interference from the matrix of TCPM [21]. Therefore, many approaches have been developed for the enrichment of AAs. Recently, magnetic solid phase extraction (MSPE) has attracted intense attention due to its excellent magnetic separation capacity. Additionally, it is available for multiple choices in detection methods at the back-end. More importantly, the shell around magnetic particles can easily be modified by different functional groups via covalent chemical reactions which ensures long term stability and efficient conjugation [22−24]. There were a few researches related to magnetic separation towards AAs detection [25−30]. Among them, most researches tended to combine magnetic particles with molecular imprinted polymers (MIPs) to ensure high selectivity [26−28], while MIPs-based adsorbents existed the drawbacks of incomplete elution of the template molecules and long equilibration time.

Inspired by the three-dimensional structure of OAT1, in which both basic amino acids and aromatic amino acids were proven to be required for transport of negatively charged substrates [31], we designed a magnetic polymeric hybrid, mimicking the effect of basic and aromatic residues of OAT1, for efficient enriching aristolochic acid I (AA I) and aristolochic acid II (AA II) in TCPM. Cationic compound with positively charged amine was a good choice for binding AAs. N, N-dimethylaminopropyl acrylamide (DMAPAm) as a typical cationic monomer was widely used for industrial and biomedical purposes, such as sludge

treatment [32], gas transport [33], protein separation [34], cell purification [35] and drug delivery [36,37]. In this study, we introduced DMAPAm on the surface of magnetic nanoparticles via polymerization in order to enhance the selectivity for AAs. After protonation of DMAPAm, the surface of the nanoparticles became hydrophilic, thus improving the compatibility of the adsorbent with the aqueous sample matrix. The single ionizable property of the polymer layer was not perfect with respect to the hydrophobicity and conjugation of the phenanthrene ring of AAs. Therefore, divinylbenzene (DVB) was copolymerized to achieve double anchors into AAs through hydrophobic and π-π interactions. Next, we applied the copolymer grafted magnetic hybrid to analyze AA I and AA II in TCPM.

2. Materials and methods

2.1. Chemicals and reagents

AA I and AA II were purchased from Sigma Aldrich (St. Louis, MO). Chlorogenic acid, ursolic acid, quercetin and berberine were from Chengdu Pufei De Biotech Co., Ltd (Chengdu, China). $FeCl_3 \cdot 6H_2O$, sodium acetate anhydrous (NaAc), trisodium citrate, tetraorthosilicate (TEOS), 3-(trimethoxysilyl) propyl methacrylate (TPM), DVB, DMAPAm, 2,2-azobisisobutyronitrile (AIBN) were obtained from Aladdin Industrial Co., Ltd (Shanghai, China). Formic acid, methanol, acetonitrile and ethylene glycol were bought from Shanghai Macklin Biochemical. Co., Ltd (Shanghai, China). The solvents listed above were of chromatographic grade.

2.2. Instrument and HPLC conditions

The morphologies of magnetic nanocomposites were observed using a SU8010 scanning electron microscope (SEM, Hitachi, Japan) and JEM 2100F transmission electron microscope (TEM, JEOL, Japan). Infrared spectra were recorded with a Nicolet 6700 FT-IR spectrophotometer (Thermo Scientific, USA). Magnetic properties were measured by a LakeShore 7404 vibrating sample magnetometry (VSM, LakeShore, USA).

Quantitative analysis was carried out with an Agilent 1260 series liquid chromatography system (Agilent Technologies, USA). A ChromCore C18 column (4.6 × 250 mm, 5 μm) was chosen for chromatographic separation. 20 μL of samples were injected into the system and eluted with mobile phase of acetonitrile (containing 0.1% formic acid)

and water (containing 0.1% formic acid). The gradient program was shown in Table S1, and the detection wavelength was set at 390 nm.

2.3. Preparation of magnetic adsorbents of MNs@SiO$_2$T-DvbDam

The MNs@SiO$_2$T-DvbDam nanocomposite was synthesized in three steps. The synthesis procedure was illustrated in Fig. 1A. Firstly, magnetic nanoparticles Fe$_3$O$_4$ (abbreviated as MNs) were prepared by solvothermal approach based on the literatures

[38]. Subsequently, the nanoparticles were coated with silica (MNs@SiO$_2$T) and then introduced with double bond (MNs@SiO$_2$T) according to previous work [39], for which TEOS was adopted as silica source, and TPM was served as a silane coupling agent. In a typical procedure of free polymerization, the functional monomer of DMAPAm and the crosslinking agent of DVB were copolymerized on the surface. MNs@SiO$_2$T-DvbDam was obtained. The overall synthetic procedure was shown in Fig. 1A and the synthetic details were in supporting information.
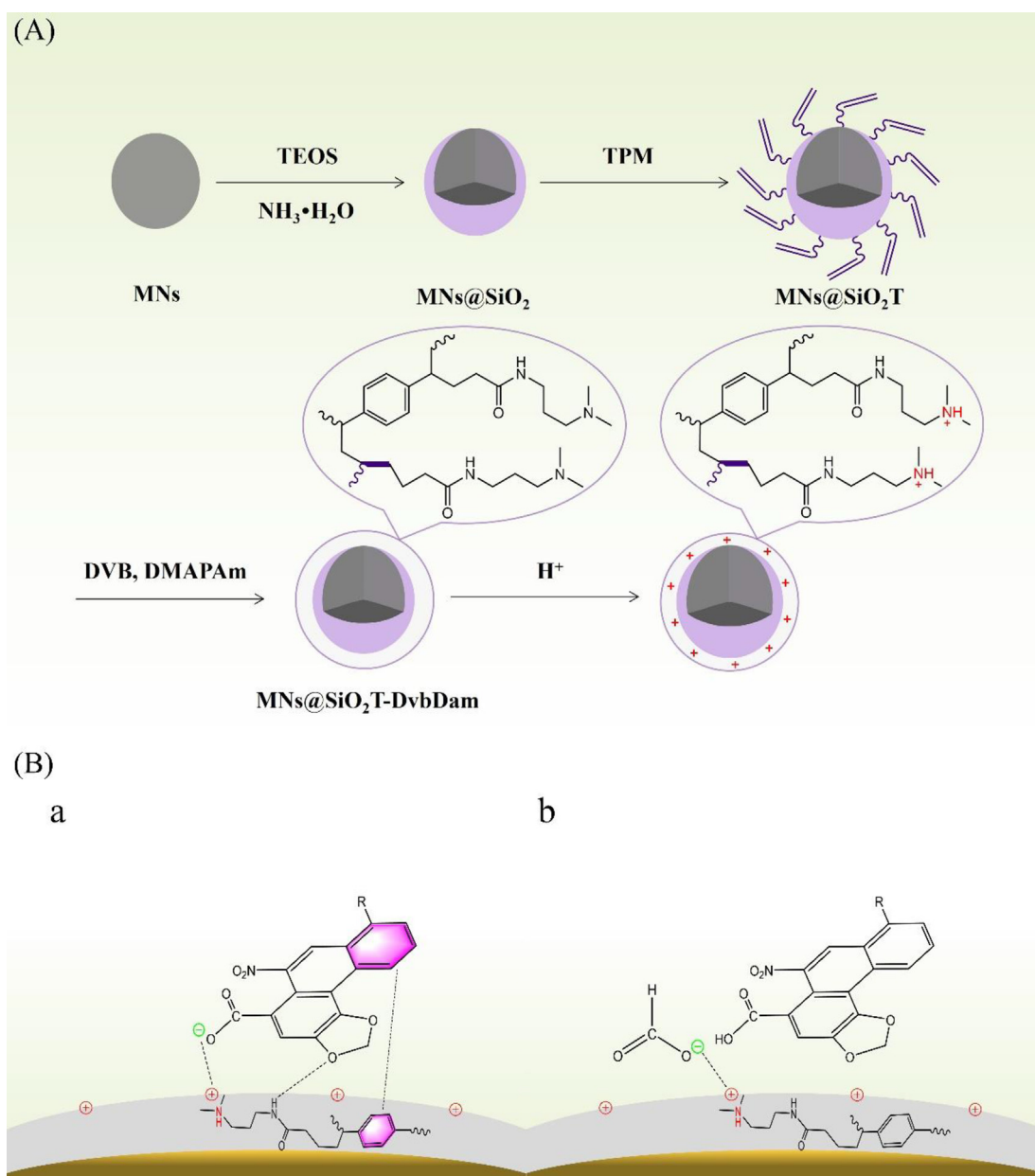

Fig. 1. (A) Synthetic scheme of MNs@SiO$_2$T-DvbDam. (B) Mechanism of action between AAs and MNs@SiO$_2$T-DvbDam in the adsorption (a) and desorption (b).

2.4. Sample preparation and MSPE procedures

1.0 g of the powder or liquid TCPM was dissolved in 20 mL of distilled water. The extracting solution was filtered and adjusted to the right pH before MSPE procedures. The details about names and forms of TCPM were presented in Table 1.

The MSPE conditions, including the amount of adsorbents, extraction time, and type of elution solvent and elution time were optimized using a spiked extracting solution of Weiyanning Keli. Then, the extracting solution (2 mL) was mixed with 5 mg of MNs@SiO$_2$T-DvbDam and shaken for 4 min. The adsorbents were quickly collected by a magnet and washed with 2 mL of water. Subsequently, 1 mL of acetonitrile containing 2% formic acid was added and the elution was performed under ultrasonication for 7 min. The eluent was evaporated to dryness under a gentle stream of nitrogen at room temperature. The residue was redissolved in acetonitrile (1 mL) and filtered through a 0.22 μm membrane prior to HPLC analysis.

2.5. Method validation

Linearity range and correlation coefficient were employed to evaluate the response linearity for the analytes. Under the optimized conditions, the working standard solution mixtures of AA I and AA II at five concentrations ranging from 0.03 to

Table 1. Results of HPLC[a] analysis of TCPM containing Xi-Xin.

Samples	Dosage forms	Content of AA I[b] (μg mL^{-1})	Content of AA II[c] (μg mL^{-1})
Biyuanshu Koufuye	Liquid	ND[d]	ND
Tongtian Koufuye	Liquid	ND	0.06
Ditongbiyan Shui	Liquid	ND	ND
Dingxiyatong Jiaonang	Capsule	ND	ND
Xinfangbiyan Jiaonang	Capsule	ND	ND
Chitongxiaoyanling Keli	Granule	ND	ND
Jiuweiqianghuo Keli	Granule	ND	ND
Weiyanning Keli	Granule	ND	ND
Xiaoqinglong Keli	Granule	0.04	ND
Xinqin Keli	Granule	ND	ND
Chuanxiongchatiao Wan	Condensed pill	ND	ND
Zhuifengtougu Wan	Condensed pill	ND	ND

[a] High performance liquid chromatography.
[b] Aristolochic acid I.
[c] Aristolochic acid II.
[d] Not detected.

2.0 μg mL^{-1} and from 0.04 to 2.0 μg mL^{-1} (n = 6), respectively, were analyzed. The calibration curves were established using the peak areas against concentrations of AA I and AA II. The limits of detection (LOD) and the limits of quantification (LOQ) were calculated by the formula of LOD = 3 (SD/S) and LOQ = 10 (SD/S), respectively, where SD was the standard deviation of the response and S was the slope of the calibration plot. Method performance was assessed by spiking with AAs at three different concentrations (0.05, 0.25 and 1.00 μg mL^{-1}) on blank TCPM samples. We chose Weiyanning Keli containing no AAs as the blank TCPM. The method precision was evaluated based on the peak areas percent relative standard deviation (%, RSD) measured through replicate analyses of the spiked samples on the same day (n = 6) and over six separate days in two weeks. The method accuracy was determined by analyzing AAs-spiked samples, and the recoveries at different concentrations were obtained by comparing the amount calculated from the calibration curves, to the nominal spike levels.

3. Results and discussion

3.1. Characterization of MNs@SiO$_2$T-DvbDam

The morphology and detailed structures of MNs and the final product MNs@SiO$_2$T-DvbDam were observed by SEM, as shown in Fig. 2A, the synthesized MNs appeared raspberry-like spheres with the average diameters of 320 nm. After coating with the silica and copolymer layer (Fig. 2B), the average size of the nanoparticles increased to approximately 390 nm, besides, the surface of spheres became smooth compared to naked Fe$_3$O$_4$ particles. To further observe the feature of MNs@SiO$_2$T-DvbDam, TEM was utilized to evaluate the coating results, from which an obvious core−shell structure and monodisperse distribution were exhibited (Fig. 2C). Two layers were observed on the surface in the image at higher magnification (Fig. 2D), the thickness was approximately 20 nm for the inner layer of SiO$_2$T and 10 nm for the outer layer of copolymers. All the electron microscopic results suggested the successful modification of copolymers on the surface of MNs.

The infrared adsorption spectroscopy was used for investigating the formation of MNs@SiO$_2$T-DvbDam. As shown in Fig. 3A, the adsorption bands at 580 cm^{-1} and 3413 cm^{-1} were attributed to Fe−O−Fe stretching of Fe$_3$O$_4$ and O−H stretching vibration of the absorbed water. The band at 1089 cm^{-1} was originated from Si−O−Si stretching
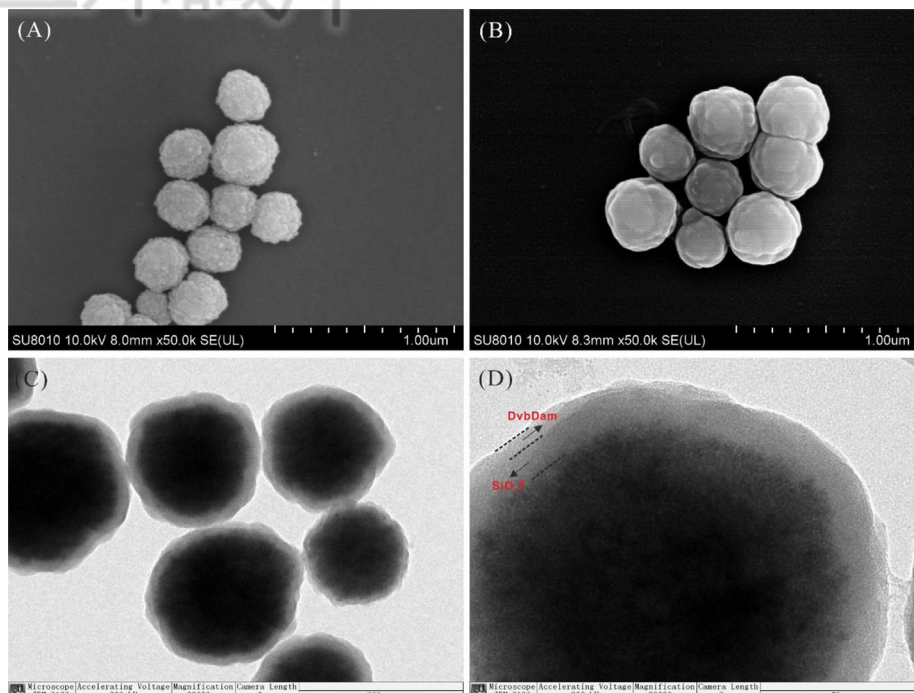
Fig. 2. The SEM images of (A) MNs and (B) MNs@SiO$_2$T-DvbDam. The TEM images of (C) MNs@SiO$_2$T-DvbDam in 20000X and (D) MNs@SiO$_2$T-DvbDam in 80000X.
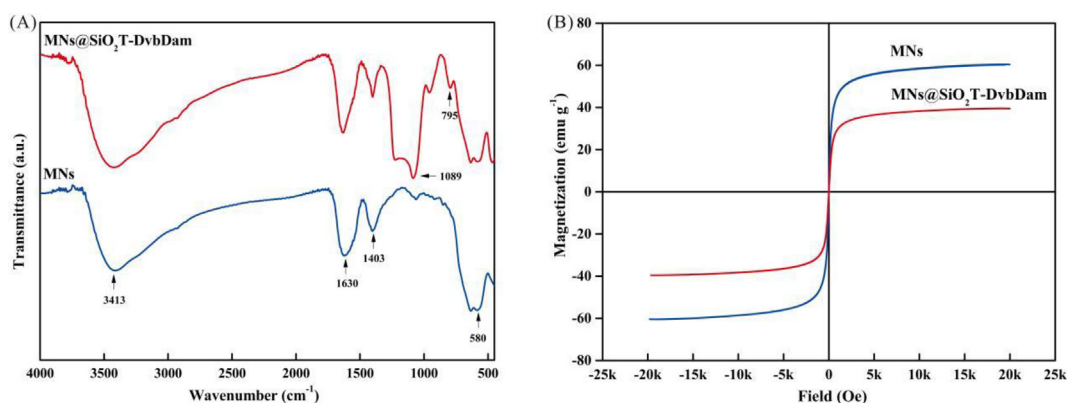

Fig. 3. FT-IR spectra of (A) MNs and MNs@SiO$_2$T-DvbDam. The hysteresis loops of (B) MNs and MNs@SiO$_2$T-DvbDam.

vibration of silica layer, which demonstrated the SiO$_2$ was coated on the surface of Fe$_3$O$_4$. The characteristic peaks of carboxylate of MNs were observed near at 1630 cm^{-1} and 1403 cm^{-1}. The adsorption band at 1630 cm^{-1} showed higher intensity and sharper shape in the spectrum of MNs@SiO$_2$T-DvbDam, compared to that in the spectrum of MNs. It was probably due to the introduction of −CONH− of DMAPAm. The peak appeared at 795 cm^{-1} which was associated with aromatic C−H bending also confirmed the formation of functional monomer layer.

The VSM was employed to investigate the magnetic properties of MNs and MNs@SiO$_2$T-DvbDam.

S-shape curves in Fig. 3B demonstrated apparent superparamagnetic behaviors for both MNs and MNs@SiO$_2$T-DvbDam because all the remanence and coercivity tended to be zero, which promised not only instant magnetic response but also fast release in the case of magnetic field withdrawal. Besides, the saturation magnetization values of MNs and MNs@SiO$_2$T-DvbDam were observed to be 60.2 emu g^{-1} and 39.6 emu g^{-1}, respectively. The magnetization decrease of MNs@SiO$_2$T-DvbDam might stem from the non-magnetic polymer layer grafted on the surface. Despite all this, the magnetization of MNs@SiO$_2$T-DvbDam is sufficient for the separation of the adsorbents from matrices.

3.2. The potential binding modes

The potential binding modes between MNs@SiO$_2$T-DvbDam and AAs were briefly demonstrated in Fig. 1B. Experiments targeting the OAT1 suggested ideal substrates were hydrophobic, might form hydrogen bonds, and had increased affinity with increased negative charge strength [31]. Similarly, in adsorption condition, the protonated tertiary amine groups on MNs@SiO$_2$T-DvbDam suggested the possibility of a binding site for negatively charged carboxyl groups on the AAs. Moreover, the aromatic groups on MNs@SiO$_2$T-DvbDam provided a hydrophobic domain and conjugate system for binding AAs. Additionally, hydrogen bond was a potential interaction between amide of MNs@SiO$_2$T-DvbDam and oxygen-containing heterocycle of AAs (Fig. 1Ba). While in desorption condition, the interactions can be broken by higher affinity with increased negative charge strength of formic acid, thus achieving the separation of AAs from the magnetic composite (Fig. 1Bb).

3.3. Capacity of MNs@SiO$_2$T-DvbDam for AAs

The adsorption capacity is defined as the maximum amount of analyte captured by MNs@SiO$_2$T-DvbDam, which is one of the crucial characteristics of an adsorbent. The capacity of the composites was evaluated by dispersing 5 mg of composites in a set of AA I or AA II solution, methanol−water (4:1, v/v, pH = 4) was used as the solvent in the binding experiment. The capacity of the composites was calculated according to the equation shown in supporting information.

The curve regression between the adsorption capacity and initial concentration of AA I and AA II was shown in Fig. 4A. The adsorption amount (defined as Q, μg mg^{-1}) of the nanocomposite for AA I was observed to increase rapidly and reach 37.30 μg mg^{-1} at 125 μg mL^{-1}. Similarly, the capacity of the nanocomposite for AA II was observed to be close to the equilibration value (36.01 μg mg^{-1}) at 125 μg mL^{-1}. These results indicated that the adsorption capacity of MNs@SiO$_2$T-DvbDam for AA I and AA II was adequate to handle trace amounts of AAs in real samples. The adsorption capacity of this work was a distinct merit compared with other materials (Table 2), which was probably ascribed to the ionizable copolymer layer and the monodispersity of the magnetic core.

3.4. Influence of pH

DMAPAm was widely employed as pH-responsive substance to be modified in the polymer backbone and on the surface of nanoparticles. The surface ionization of the adsorbent depends on the pH of the matrix. Therefore, broad ranges of pH value from 3 to 11 were examined. As shown in Fig. 4B, high error bars were recorded at pH = 3, which was mainly due to the decrease of the solubility of AA I and AA II under this circumstance. The partial precipitation of AAs destroyed the homogeneity of reaction solution. Then, a high recovery was observed at pH = 4 and it declined gradually as the pH value increased from 4 to 8. There was a dramatic decline when pH value was over 8 for both analytes, probably due to the enhanced electrostatic repulsion between the proposed nanocomposite and AAs in basic solution. Therefore, weak acidic solution was favorable to the adsorption of AAs and we finally fixed 4 as the optimum pH value for the following experiments.

3.5. Selectivity of the nanocomposites

To investigate the selectivity of the proposed nanocomposite, six compounds naturally occurring in medical plants including AA I, AA II, chlorogenic
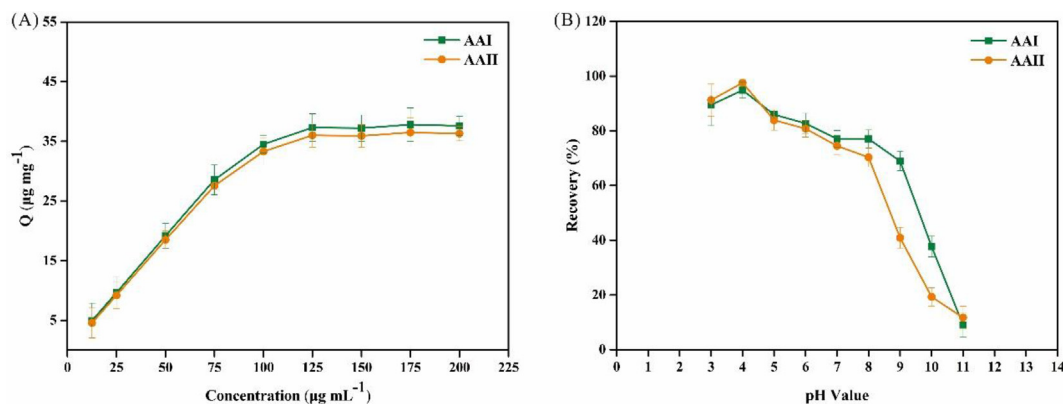

Fig. 4. Adsorption capacities of (A) MNs@SiO$_2$T-DvbDam. (B) Influences of pH on recovery.

Table 2. Comparison of present method with other reported methods.

Samples	Adsorbents	Extraction time (min)	Magnetic properties (emu g^{-1})	Analytes	LOD (μg mL^{-1})	Adsorption capacity (μg mg^{-1})	Refs
Rat urine	MMC@MIPs	30	18.1	AA I[a]	0.03	8.65	[26]
Rat urine	MMC@MIPs	30	18.1	AA II[b]	0.17	9.30	[26]
TCM[c]	MCNTs@AAI-MIPs	15	45.56	AA I	0.034	18.54	[27]
TCM	TMMIPs	30	n.d.a[e]	AA I	0.02667	8.51	[28]
TCM	CNT/Fe$_3$O$_4$@SiO$_2$-A	30	2.5	AA I	0.05	24.50	[29]
TCM	CNT/Fe$_3$O$_4$@SiO$_2$-A	30	2.5	AA II	0.025	n.d.a	[29]
TCM	Fe$_3$O$_4$@SiO$_2$-TPM@StVp	7	39.4	AA I	0.05	n.d.a	[30]
TCPM[d]	MNs@SiO$_2$T-DvbDam	4	39.6	AA I	0.009	37.30	This work
				AA II	0.013	36.01	

[a] Aristolochic acid I.
[b] Aristolochic acid II.
[c] Traditional Chinese medicine.
[d] Traditional Chinese patent medicines.
[e] No data available.

acid, ursolic acid, quercetin and berberine were tested using MNs@SiO$_2$T-DvbDam. The chemical structures of the six substances were shown in Table S2 and the results were shown in Fig. 5. The adsorption behavior of the proposed nanocomposite for AA I and AA II were similar because of the semblable carboxyl groups, hydrophobicity and conjugated system. The composite demonstrated a lower adsorption capacity for substances bearing carboxyl groups while lack of hydrophobicity (chlorogenic acid) or without conjugated system (ursolic acid). The adsorption capacity for substances without carboxyl groups including quercetin and berberine were much lower than that for AAs, especially for berberine, which possessed electrostatic repulsion and weak hydrophobicity to the magnetic composite. It can be deduced that the cationic moiety, the hydrophobicity and conjugated system of the copolymer layer resulted in the high

selectivity of MNs@SiO$_2$T-DvbDam for AAs due to multiple interactions. Therefore, MNs@SiO$_2$T-DvbDam was used for the following experiments.

3.6. Optimization for MSPE procedure

To obtain excellent extraction efficiency, the main parameters were investigated, including amount of adsorbents, adsorption time, type of elution solvent, and elution time. As MNs@SiO$_2$T-DvbDam exhibited the similar selectivity and adsorption capacity for AA I and AA II, the optimization of MSPE conditions was conducted between AA I and the nanocomposites. The results were presented in Fig. S1.

The amount of adsorbents and adsorption time exerted a great influence on extraction efficiency of the target compound. In this study, the amounts of adsorbents from 1.0 to 20 mg and the adsorption time in the range of 2−8 min were investigated. The extraction was performed as described in section 2.4. As shown in Fig. S1a and S1b, the recovery increased to 90.6% when 5 mg MNs@SiO$_2$T-DvbDam was consumed, and then it barely changed with the increase of adsorbents. The highest recovery of 98.2% for AA I was acquired when the extracting time reach to 4 min. Hence, the optimal adsorbent amount of 5 mg and adsorption time of 4 min were selected for subsequent experiments.

A reasonable elution solvent is beneficial to obtain the excellent elution capability. The most important factor to be taken into consideration is the polarity of AA I. Methanol and acetonitrile were investigated. In view of the electrostatic interaction between AA I and the adsorbent, we take advantage of formic acid to occupy the binding sites on the adsorbents to elute AA I. As shown in Fig. S1c, higher recoveries were recorded when eluting by acetonitrile compared to methanol. After addition of formic
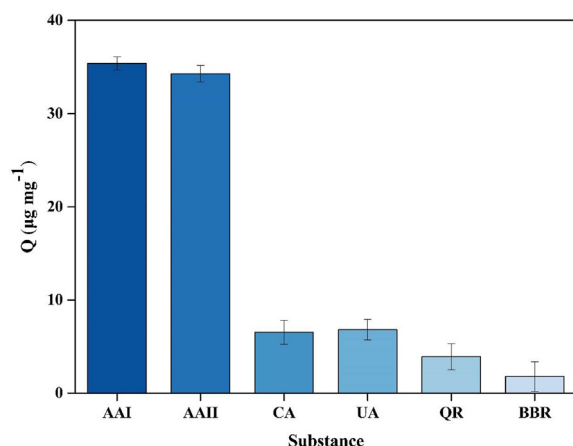

Fig. 5. Selective adsorption capacities of MNs@SiO$_2$T-DvbDam for AAs: AA I, aristolochic acid I; AA II, aristolochic acid II; CA, chlorogenic acid; UA, ursolic acid; QR, quercetin; BBR, berberine.

acid in methanol (v/v, 2%) and acetonitrile (v/v, 2%), the elution efficiencies were both improved obviously. In particular, the recovery obtained by acetonitrile containing 2% formic acid has risen to 96.3%. Therefore, the formic acid in acetonitrile (v/v, 2%) was chosen for the optimal elution solvent. The elution time is a key parameter in determining the final analytes concentration before HPLC analysis. The time of 3, 5, 7 and 9 min was tested. It can be seen from Fig. S1d that the recovery increased to be the highest at elution time of 7 min and reached an equilibrium. As a consequence, 7 min was optimal time in elution process.

3.7. Method validation

Method validations including linearity, sensitivity, accuracy and precision were studied under the optimized pretreatment conditions.

Linearity range and correlation coefficient were employed to evaluate the response linearity for the analytes. Under the optimized conditions, the working standard solution mixtures of AA I and AA II at five concentrations ranging from 0.03 to 2.0 μg mL^{-1} and from 0.04 to 2.0 μg mL^{-1} (n = 6), respectively, were analyzed. The calibration curves were established using the peak areas against concentrations of AA I and AA II. The limits of detection (LOD) and the limits of quantification (LOQ) were calculated by the formula of LOD = 3 (SD/S) and LOQ = 10 (SD/S), respectively, where SD was the standard deviation of the response and S was the slope of the calibration plot. The results of linearity and sensitivity were listed in Table S3. Analytical responses were found to be linear, with r^2 value greater than 0.9990 for both AA I and AA II. the LOD and LOQ for AA I were 0.009 μg mL^{-1} and 0.03 μg mL^{-1}, and for AA II were 0.013 μg mL^{-1} and 0.04 μg mL^{-1}, respectively.

Method performance was assessed by spiking with AAs at three different concentrations (0.05, 0.25, and 1.00 μg mL^{-1}) on blank TCPM samples. The method precision was evaluated based on the peak areas percent relative standard deviation (%, RSD) measured through replicate analyses of the spiked samples on the same day (n = 6) and over six separate days in two weeks. The method accuracy was determined by analyzing AAs-spiked samples, and the recoveries at different concentrations were obtained by comparing the amount calculated from the calibration curves, to the nominal spike levels. The recoveries were in the range of 90.4−98.9% at the three spiking levels, the intra- and inter-day RSDs were less than 2.9%, indicating that the obtained recoveries and

precisions were acceptable. All above results were summarized in Table S3.

3.8. Analysis of the real samples

The validated method was then applied to detect AA I and AA II in TCPM containing Xi-Xin. A total of 12 samples were collected from pharmacy in Chengdu of China. Among them, AA I was detected in a single sample at the concentration of 0.04 μg mL^{-1}, which is close to the LOQ of the AA I. Meanwhile, AA II was found in one sample at the concentration of 0.06 μg mL^{-1}, which is near the LOQ for the AA II too (Table 1). It is important evidence that the toxic components of Chinese herbal medicines have been reduced and controlled after standardization of the use of Aristolochic and Asarum herbs. In order to evaluate the performance of MNs@SiO$_2$T-DvbDam for AA I and AA II in the real samples, 2.0 mL spiked sample solution containing 1.0 μg mL^{-1} AA I and AA II was analyzed under the optimal conditions. The chromatograms were displayed in Fig. 6. The intensity of AA I or AA II extracted from the spiked sample solution was almost the same as that in the standard solution, while the intensity of interferences decreased significantly after extraction, indicating that AA I and AA II were enriched effectively through our proposed strategy.

3.9. Reusability of the adsorbent

The reusability is a key factor to evaluate the performance of adsorbents. The MNs@SiO$_2$T-DvbDam was washed by acetonitrile containing 2%
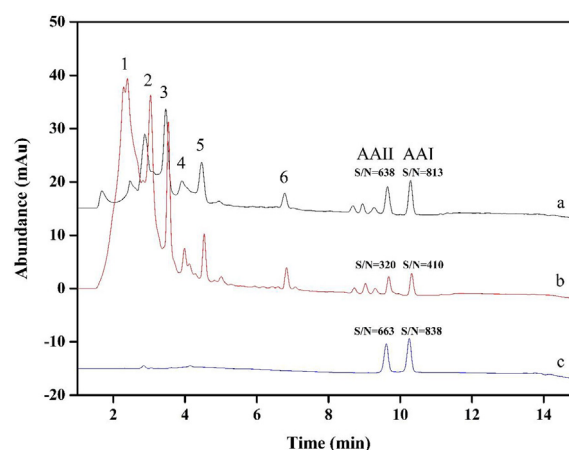

Fig. 6. Chromatograms of Weiyanning Keli samples spiked with AA I and AA II at 1.0 μg mL^{-1}. (a) Spiked sample after MSPE; (b) Spiked sample before MSPE; (c) Standard solution of AA I and AA II. Attenuated peaks: 1, 2, 3, 4, 5 and 6.

formic acid and dried in 60 °C vacuum each time before next use. Fig. S2 displayed the recoveries of AA I and AA II were remained over 90% in five consecutive adsorption−desorption cycles, but in the sixth time the recovery decreased to 84.6% and 81.1% for AA I and AA II, respectively, which was mainly due to the irreversible adsorption and the partial destruction of adsorption sites during the washing procedure. The above results highlighted the merits of good stability and satisfactory reusability for the proposed materials.

3.10. Comparison with other materials and methods

The comparative studies were conducted among four adsorbents with the same architecture including MNs, MNs@SiO$_2$T, MNs@SiO$_2$T-DvbDam, Fe$_3$O$_4$@-silica@copolymer. Among them, MNs and MNs@SiO$_2$T were the intermediate for making MNs@SiO$_2$T-DvbDam, Fe$_3$O$_4$@silica@copolymer coated with poly (DVB-co-NVP) layer was synthesized in our previous work [39]. Fig. S3 displayed that MNs@SiO$_2$T-DvbDam had the highest recoveries for both AA I and AA II, while recoveries of MNs, MNs@SiO$_2$T and Fe$_3$O$_4$@silica@copolymer for both were less than 35%, indicating that the grafted copolymers contributed to the adsorption of AAs.

The analytical performance of the MNs@SiO$_2$T-DvbDam for AAs detection was compared to most of MSPE-HPLC methods reported previously [26−30]. As listed in Table 2, the adsorption capacity of this work is a distinct merit compared with other materials, which is probably ascribed to the ionizable copolymer layer and the monodispersity of the magnetic core. The LOD of this method is lower than that of other MSPE-HPLC methods, while this advantage is not significant in terms of sensitivity. We also compared the magnetic properties and adsorption time MNs@SiO$_2$T-DvbDam had a better magnetic properties than MMC@MIPs (18.1 emu g^{-1}) [26] and CNT/Fe$_3$O$_4$@SiO$_2$-A (2.5 emu g^{-1}) [29], shorter adsorption time than any other magnetic composites.

4. Conclusion

In summary, inspired by the mechanism of AAs-induced nephrotoxicity, we design a magnetic polymeric nanostructure using monodispersed magnetic silicon sphere to bear basic and aromatic copolymer on the surface, and thus produce a desirable ionization effect and also an amphiphilic property. The pH-responsive monomer of DMA-PAm was employed for the first time to be polymerized on the surface of magnetic nano-composite and the extraction efficiencies of the obtained nanocomposite for AAs were confirmed pH sensitive. Owing to the merits of ionizable property, hydrophility/hydrophobicity, monodispersity and magnetic responsiveness, MNs@SiO$_2$T-DvbDam exhibited excellent selectivity, sensitivity, reusability and rapidity towards the enrichment of AAs in TCPM. The high simultaneous extraction capacity endowed MNs@SiO$_2$T-DvbDam with a potent tool for AAs analysis in quality management and control of TCM. In this work, we only mimicked the function of active amino acids of OATs that played key roles in AAs transport, noticeably, a putative active cavity of OATs where the key amino acids located, possibly producing an impact on substrate binding. The future work could be focused on the bionic design of the three-dimensional structure of OATs to construct novel magnetic hybrids for extract AAs with higher selectivity and sensitivity.

Conflicts of interest

The authors declare that they have no known competing financial interests or personal relationships that could have appeared to influence the work reported in this paper.

Acknowledgment

Appendix

Supporting Information

1. Experimental information

1.1 Preparation of MNs@ SiO$_2$T-DvbDam. MNs, MNs@SiO$_2$ nanoparticles were synthesized according to a previous report [39]. Next, 500 mg MNs@SiO$_2$ was dispersed in 200 mL of ethanol and 1.5 mL of TPM was added. The reaction was kept at 60 °C for 12 h. The nanoparticles coated with silica and TPM (MNs@SiO$_2$T) turned to brown.

They were thoroughly rinsed with ethanol and transferred into a round-bottomed flask containing 200 mL of acetonitrile and then in 0.5 h ultrasonication. In a typical procedure of polymerization, 1 mL of DVB, 3 mL of DMAPAm and 0.5 g of AIBN were added in the flask, the mixture was placed in a water bath heated to 70 °C, and stirred for 16 h. The obtained product was named as MNs@SiO$_2$T-DvbDam and washed with DMSO and ethanol, finally dried in a vacuum oven.

1.2 Capacity of MNs@SiO$_2$T-DvbDam for AAs. The capacity of the composites was evaluated by dispersing 5 mg of composites in a set of AA I or AA II solution, and the methanol−water (4:1, v/v,

pH = 4) was used as the solvent in the binding experiment. The capacity of the composites was calculated according to the following equation:

$$Q = (C_0 - C_e) \, V/m$$

Q ($\mu g \, mg^{-1}$): adsorption amount; C_0 ($\mu g \, mL^{-1}$): initial concentration of analyte; C_e ($\mu g \, mL^{-1}$): equilibrium concentration of analyte; V (mL): volume of analyte solution; and m (mg): amount of nanocomposites.
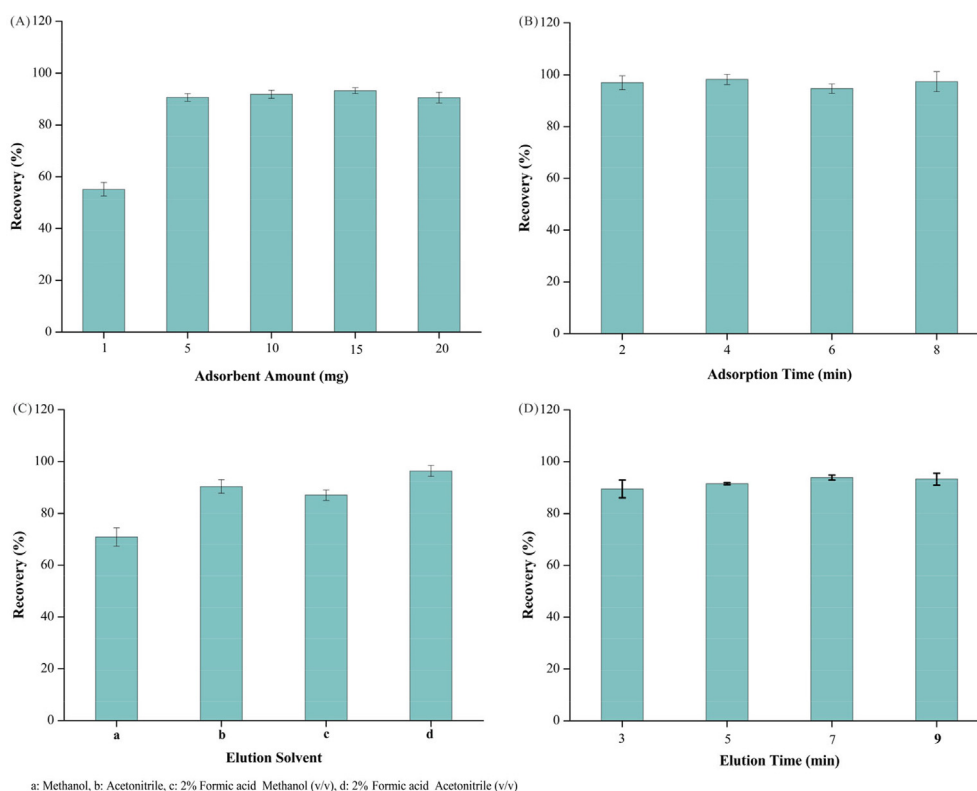
2. Results

Fig. S1. Optimization of MSPE process using AA I as a representative. (A) Adsorbent amount. (B) Adsorption time. (C) Elution solvent. (D) Elution time.
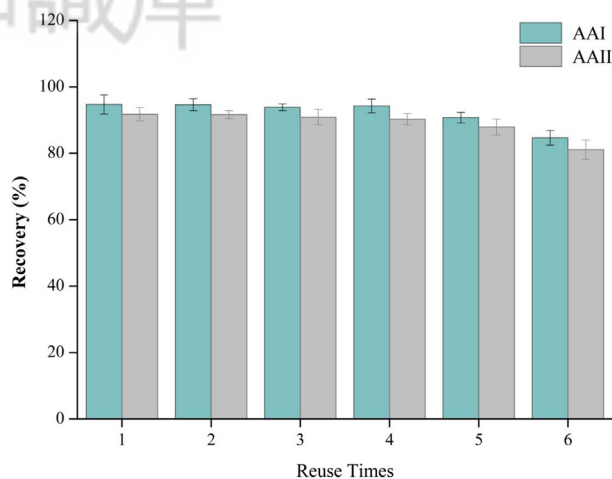
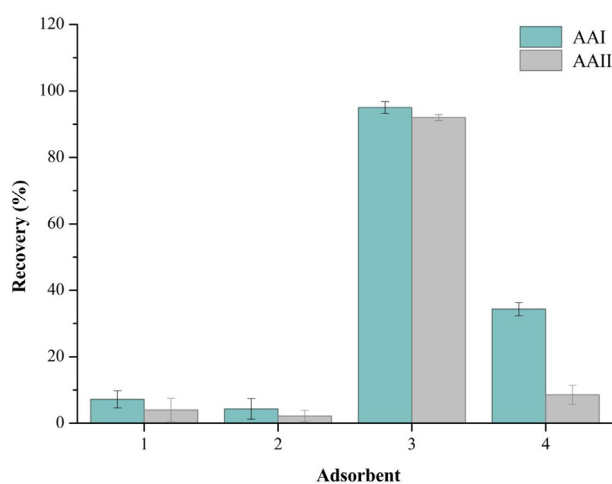*Fig. S2. Reusability of MNs@SiO₂T-DvbDam.*

Fig. S3. The extraction efficiency of four different materials for AAs. (1) MNs, (2) MNs@SiO₂T, (3) MNs@SiO₂T-DvbDam, (4) Fe₃O₄@silica@copolymer.

Table S1. The elution program in HPLC analysis.

Time (min)	Mobile phase A[a] (%)	Mobile phase B[b] (%)
0	60	40
12.0	24	76
15.0	5	95
17.0	5	95
18.0	60	40
37.0	60	40

[a] Water (containing 0.1% formic acid).
[b] Acetonitrile (containing 0.1% formic acid).

Table S2. Chemical structures and corresponding formulas used for selectivity evaluation.
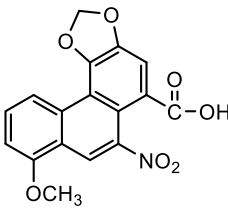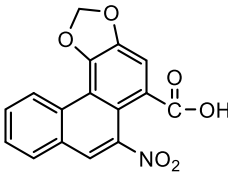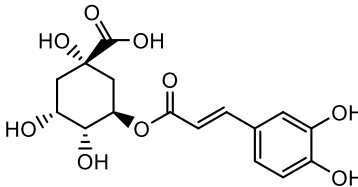
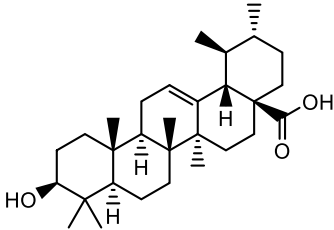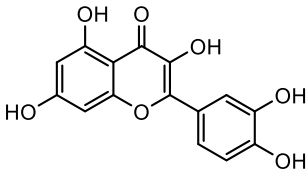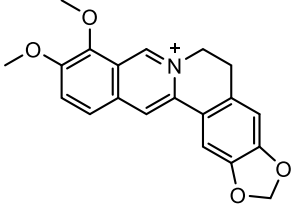| Name	Formula	Structure
Aristolochic acid I	$C_{17}H_{11}NO_7$	
Aristolochic acid II	$C_{16}H_9NO_6$	
Chlorogenic acid	$C_{16}H_{18}O_9$	
Ursolic acid	$C_{30}H_{48}O_3$	
Quercetin	$C_{15}H_{10}O_7$	
Berberine	$C_{20}H_{18}NO_4^+$	

Table S3. The validation results of the proposed strategy for determination of AAs.

Analytes	Linear range (µg mL⁻¹)	Correlation coefficients (r²)	LOD (µg mL⁻¹)	LOQ (µg mL⁻¹)	Recovery (n = 6) at three concentration (µg mL⁻¹)			Precision (RSD, %) (n = 6) at three concentration (µg mL⁻¹)					
					0.05	0.25	1.00	0.05		0.25		1.00	
								intra-day	inter-day	intra-day	inter-day	intra-day	inter-day
AA I	0.03–2.00	0.9997	0.009	0.03	90.4	98.9	91.5	1.9	2.7	1.3	2.6	0.4	2.2
AA II	0.04–2.00	0.9990	0.013	0.04	91.2	94.9	95.6	2.4	2.9	1.8	2.7	1.6	2.5

References

[1] Cronin AJ, Maidment G, Cook T, Kite GC, Simmonds MSJ, Pusey CD, et al. Aristolochic acid as a causative factor in a case of Chinese herbal nephropathy. Nephrol Dial Transplant 2002;17:524—5.

[2] Heinrich M, Chan J, Wanke S, Neinhuis C, Simmonds MSJ. Local uses of Aristolochia species and content of nephrotoxic aristolochic acid 1 and 2—a global assessment based on bibliographic sources. J Ethnopharmacol 2009;125:108—44.

[3] Zhang YF, Han YH, Dong CL, Li C, Liang T, Ling GN, et al. Rapid characterization and pharmacokinetic study of aristolochic acid analogues using ion mobility mass spectrometry. Anal Bioanal Chem 2021;413:4247—53.

[4] Arlt VM, Stiborova M, Brocke JV, Simoes ML, Lord GM, Nortier JL, et al. Aristolochic acid mutagenesis: molecular clues to the aetiology of Balkan endemic nephropathy-associated urothelial cancer. Carcinogenesis 2007;28:2253—61.

[5] Michl J, Ingrouille MJ, Simmonds MSJ, Heinrich M. Naturally occurring aristolochic acid analogues and their toxicities. Nat Prod Rep 2014;31:676—93.

[6] Chan W, Pavlovic NM, Li WW, Chan C-K, Liu JJ, Deng KL, et al. Quantitation of aristolochic acids in corn, wheat grain, and soil samples collected in Serbia: identifying a novel exposure pathway in the etiology of Balkan endemic nephropathy. J Agric Food Chem 2016;64:5928—34.

[7] Shen Q-Q, Wang J-J, Debmalya R, Sun L-X, Jiang Z-Z, Zhang L-Y, et al. Organic anion transporter 1 and 3 contribute to traditional Chinese medicine-induced nephrotoxicity. Chin J Nat Med 2020;18:196—205.

[8] Zou SS, Li JR, Zhou HB, Frech C, Jiang XL, Chu JSC, et al. Mutational landscape of intrahepatic cholangiocarcinoma. Nat Commun 2014;5:5696.

[9] Wheeler DA, Roberts LR. Comprehensive and integrative genomic characterization of hepatocellular carcinoma. Cell 2017;169:1327—41.

[10] Chen Y-Y, Chung J-G, Wu H-C, Bau D-T, Wu K-Y, Kao S-T, et al. Aristolochic acid suppresses DNA repair and triggers oxidative DNA damage in human kidney proximal tubular cells. Oncol Rep 2010;24:141—53.

[11] Martena MJ, van der Wielen JCA, van de Laak LFJ, Konings EJM, de Groot HN, Rietjens IMCM. Enforcement of the ban on aristolochic acids in Chinese traditional herbal preparations on the Dutch market. Anal Bioanal Chem 2007;389:263—75.

[12] Debelle FD, Vanherweghem JL, Nortier JL. Aristolochic acid nephropathy: a worldwide problem. Kidney Int 2008;74:158—69.

[13] Liu SY, Xian Z, Zhao Y, Wang LM, Tian JZ, Pan C, et al. Quantitative determination and toxicity evaluation of aristolochic acid analogues in Asarum heterotropoides F. Schmidt (Xixin) and traditional Chinese patent medicines. Front Pharmacol 2021;12:761593.

[14] Fu XF, Liu Y, Li W, Bai Y, Liao YP, Liu HW. Determination of dissociation constants of aristolochic acid I and II by capillary electrophoresis with carboxymethyl chitosan-coated capillary. Talanta 2011;85:813—5.

[15] Agrawal P, Laddha K. Development of validated high-performance thin layer chromatography for quantification of aristolochic acid in different species of the Aristolochiaceae family. J Food Drug Anal 2017;25:425—9.

[16] Ouyang L, Zhang Q, Ma G, Zhu LH, Wang YQ, Chen ZL, et al. New dual-spectroscopic strategy for the direct detection of aristolochic acids in blood and tissue. Anal Chem 2019;91:8154—61.

[17] Oraby HF, Alarfaj NA, El-Tohamy MF. Gold nanoparticle-enhanced luminol/ferricyanide chemiluminescence system for aristolochic acid-I detection in medicinal plants and slimming products. Green Chem Lett Rev 2017;10:138—47.

[18] Yuan JB, Nie LH, Zeng DY, Luo XB, Tang F, Ding L, et al. Simultaneous determination of nine aristolochic acid analogues in medicinal plants and preparations by high-performance liquid chromatography. Talanta 2007;73:644—50.

[19] Koh HL, Wang H, Zhou S, Chan E, Woo SO. Detection of aristolochic acid I, tetrandrine and fangchinoline in medicinal plants by high performance liquid chromatography and liquid chromatography/mass spectrometry. J Pharm Biomed Anal 2006;40:653—61.

[20] Zhang JH, Wang YN, Sun J, Zhou GW, Jiang XJ, Wang XK. QuEChERS pretreatment combined with high-performance liquid chromatography-tandem mass spectrometry for determination of aristolochic acids I and II in Chinese herbal patent medicines. RSC Adv 2020;10:25319—24.

[21] Fan Y, Li ZM, Xi J. Recent developments in detoxication techniques for aristolochic acid-containing traditional Chinese medicines. RSC Adv 2020;10:1410—25.

[22] Yilmaz E, Sarp G, Uzcan F, Ozalp O, Soylak M. Application of magnetic nanomaterials in bioanalysis. Talanta 2021;229: 122285.

[23] Yu X, Zhong T, Zhang YJ, Zhao XH, Xiao Y, Wang L, et al. Design, preparation, and application of magnetic nanoparticles for food safety analysis: a review of recent advances. J Agric Food Chem 2022;70:46—62.

[24] Wang Y, Yang XM, Pang L, Geng PF, Mi F, Hu CM, et al. Application progress of magnetic molecularly imprinted polymers chemical sensors in the detection of biomarkers. Analyst 2022;147:571—86.

[25] Ansari S, Masoum S. A multi-walled carbon nanotube-based magnetic molecularly imprinted polymer as a highly selective sorbent for ultrasonic-assisted dispersive solid-phase microextraction of sotalol in biological fluids. Analyst 2018; 143:2862—75.

[26] Ge Y-H, Shu H, Xu X-Y, Guo P-Q, Liu R-L, Luo Z-M, et al. Combined magnetic porous molecularly imprinted polymers and deep eutectic solvents for efficient and selective extraction of aristolochic acid I and II from rat urine. Mater Sci Eng C 2019;97:650—7.

[27] Li F, Gao J, Li XX, Li YJ, He XW, Chen LX, et al. Preparation of magnetic molecularly imprinted polymers functionalized carbon nanotubes for highly selective removal of aristolochic acid. J Chromatogr A 2019;1602:168—77.

[28] Xiong HH, Fan Y, Mao XJ, Guo L, Yan AP, Guo X, et al. Thermosensitive and magnetic molecularly imprinted polymers for selective recognition and extraction of aristolochic acid I. Food Chem 2022;372:131250.

[29] Shu H, Chen GN, Wang L, Cui X, Wang Q, Li W, et al. Adenine-coated magnetic multiwalled carbon nanotubes for the selective extraction of aristolochic acids based on multiple interactions. J Chromatogr A 2020;1627:461382.

[30] Ji FQ, Jin RR, Luo C, Deng CH, Hu YM, Wang L, et al. Fast determination of aristolochic acid I (AAI) in traditional Chinese medicine soup with magnetic solid-phase extraction by high performance liquid chromatography. J Chromatogr A 2020;1609:460455.

[31] Perry JL, Dembla-Rajpal N, Hall LA, Prltchard JB. A three-dimensional model of human organic anion transporter 1. J Biol Chem 2006;281:38071—9.

[32] Sakohara S, Yagi S, Iizawa T. Dewatering of inorganic sludge using dual ionic thermosensitive polymers. Sep Purif Technol 2011;80:148—54.

[33] Saedi S, Madaeni SS, Seidi F, Shamsabadi AA, Laki S. Fixed facilitated transport of CO_2 through integrally-skinned asymmetric polyethersulfone membrane using a novel synthesized poly (acrylonitrile-Co-N, N-dimethylaminopropyl acrylamide). Chem Eng J 2014;236:263—73.

[34] Nagase K, Kitazawa S, Yamada S, Akimoto AM, Kanazawa H. Mixed polymer brush as a functional ligand of silica beads for temperature-modulated hydrophobic and electrostatic interactions. Anal Chim Acta 2020;1095: 1—13.

[35] Nagase K, Hatakeyama Y, Shimizu T, Matsuura K, Yamato M, Takeda N, et al. Thermoresponsive cationic copolymer brushes for mesenchymal stem cell separation. Biomacromolecules 2015;16:532—40.

[36] Nakayama Y. Hyperbranched polymeric "star vectors" for effective DNA or siRNA delivery. Acc Chem Res 2012;45: 994—1004.

[37] Richter F, Martin L, Leer K, Moek E, Hausig F, Brendel JC, et al. Tuning of endosomal escape and gene expression by functional groups, molecular weight and transfection medium: a structure-activity relationship study. J Mater Chem B 2020;8:5026—41.

[38] Liu J, Sun ZK, Deng YH, Zou Y, Li CY, Guo XH, et al. Highly water-dispersible biocompatible magnetite particles with low cytotoxicity stabilized by citrate groups. Angew Chem 2009;48:5989—93.

[39] Xu M, Liu MH, Sun MR, Chen K, Cao XJ, Hu YM. Magnetic solid-phase extraction of phthalate esters (PAEs) in apparel textile by core-shell structured Fe_3O_4@silica@triblock-copolymer magnetic microspheres. Talanta 2016;150: 125—34.